BJR

https://doi.org/10.1259/bjr.20220357

Received: 01 April 2022 | Revised: 25 June 2022 | Accepted: 12 August 2022 | Published online: 08 September 2022

Cite this article as:
Daube-Witherspoon ME, Pantel AR, Pryma DA, Karp JS. Total-body PET: a new paradigm for molecular imaging. *Br J Radiol* (2022) 10.1259/bjr.20220357.

REVIEW ARTICLE

Total-body PET: a new paradigm for molecular imaging

MARGARET E DAUBE-WITHERSPOON, AUSTIN R PANTEL, DANIEL A PRYMA and JOEL S KARP

Department of Radiology, University of Pennsylvania, Philadelphia, United States

Address correspondence to: Professor Joel S Karp
E-mail: *joelkarp@pennmedicine.upenn.edu*

ABSTRACT

Total body (TB) positron emission tomography (PET) instruments have dramatically changed the paradigm of PET clinical and research studies due to their very high sensitivity and capability to image dynamic radiopharmaceutical distributions in the major organs of the body simultaneously. In this manuscript, we review the design of these systems and discuss general challenges and trade-offs to maximize the performance gains of current TB-PET systems. We then describe new concepts and technology that may impact future TB-PET systems. The manuscript summarizes what has been learned from the initial sites with TB-PET and explores potential research and clinical applications of TB-PET. The current generation of TB-PET systems range in axial field-of-view (AFOV) from 1 to 2 m and serve to illustrate the benefits and opportunities of a longer AFOV for various applications in PET. In only a few years of use these new TB-PET systems have shown that they will play an important role in expanding the field of molecular imaging and benefiting clinical practice.

INTRODUCTION

Total body (TB) PET instruments have dramatically changed the scope of PET clinical and research studies. We consider TB-PET instruments to be those with an axial field of view (AFOV) of at least 60 cm so that these instruments not only have very high sensitivity compared with instruments of standard AFOV (<30 cm), but also have the capability to image dynamic radiopharmaceutical distributions in the major organs of the body simultaneously. TB-PET instruments have only been in use since 2018 and have generated much interest in that short time in both clinical and research settings. In this manuscript, we review the design and performance of these systems, noting common features, as well as differences. We also discuss general challenges and trade-offs to maximize the performance gains of TB-PET systems. We consider these new instruments to be the first generation of a new category of PET design and discuss some areas where we expect improvements and refinements in the coming years. The manuscript then summarizes what has been learned from the initial sites with TB-PET and explores potential research and clinical applications of TB-PET.

Existing systems

The general design features and performance characteristics of the three TB-PET systems in routine use are summarized in Table 1. United Imaging (UI) Healthcare's uEXPLORER scanner with a 194 cm AFOV initiated human imaging at the University of California-Davis in 2019[4] and at several sites in China.[5] The PennPET Explorer system was built as a scalable system and was installed with a 64 cm AFOV (three rings) at the University of Pennsylvania in 2018[6] ; it now has a 142 cm AFOV (six rings). In 2020, Siemens introduced the Biograph Vision Quadra scanner with an AFOV of 106 cm.[7] The number of installations of TB-PET systems is quickly approaching two dozen, almost equally split between Siemens (mostly in Europe) and UI Healthcare (mostly in China). All three TB-PET systems use LSO or L(Y)SO crystals coupled to silicon photomultipliers (SiPMs), similar to systems with standard AFOV, with differences in the size and coupling configuration of crystals to SiPMs contributing to the differences in spatial and time-of-flight (TOF) resolutions noted in Table 1.[1–3] It is known that the TOF resolution translates to an effective gain in sensitivity, where the TOF sensitivity gain is inversely proportional to the TOF resolution[8] ; the TOF sensitivity gain should be combined with the gain in geometric sensitivity in comparing overall performance of TB-PET systems.

Sensitivity gain

The dramatic increase in sensitivity due to the long axial coverage is shown schematically in Figure 1(a). As the axial acceptance angle θ increases with the AFOV, more events at oblique axial angles are detected (events that are lost

Table 1. Design and performance of existing TB-PET systems

System	United Imaging uEXPLORER[1]	PennPET Explorer[2]	Siemens Biograph Vision Quadra[3]
Crystal size	2.76 × 2.76 × 18.1 mm^3	3.86 × 3.86 × 19 mm^3	3.2 × 3.2 × 20 mm^3
Crystals : SiPM	10.5:1	1:1	5:1
AFOV (cm)	194	142	106
Ring diameter (cm)	78.6	76.4	78.0
Axial acceptance angle Max Ring Difference	± 57°	± 62°	± 18° / ± 52° MRD 85/322
Coincidence timing window (ns)	4.5–6.9 (varies with detector unit difference)	4.5	4.7
TOF resolution (ps)	505	240	225/230 MRD 85/322
Spatial resolution @ctr			
Transverse (mm)	3.0	4.0	3.3
Axial (mm)	2.8	4.0	3.8 (MRD 85)

AFOV, axial field of view; TB-PET, total body positron emission tomography; TOF, time-of flight.

in scanners with a standard AFOV). Total sensitivity increases up to 32x in air can be achieved for the longest TB-PET system compared with standard systems. The peak sensitivity gain for a point source (or organ) reaches a maximum of about 2–3x in air (Figure 1(b)); because oblique coincidences are preferentially attenuated due to their longer pathlength through the patient,[9] however, the peak sensitivity gain in patients is less than 2x for AFOVs > 100 cm (Figure 1(c) and (d)). However, as also seen in Figure 1, with a longer AFOV comes a longer region of peak sensitivity.

There are trade-offs, however, in accepting all possible oblique events to obtain this high sensitivity. More background (random and scattered) events are detected with the larger acceptance angle, in addition to the true coincidences. These unwanted events must be corrected to obtain quantitatively accurate images. In addition, oblique events suffer from parallax errors caused by uncertainty about the depth of interaction (DOI) of the 511-keV annihilation photons in the crystal, which degrades the axial resolution at the center of the system.[10] With the PennPET Explorer, we reported a degradation in axial resolution of ~0.5 mm in the center of the AFOV[2] ; we note that this is considerably smaller than the degradation in radial resolution with increasing radial offset that also results from parallax errors and is seen in all scanners. The PennPET Explorer operates with a wide-open acceptance angle θ = ±62˚, while the uEXPLORER limits θ to ±57˚ and the Quadra currently limits θ to ±18˚ for clinical imaging. While the trade-offs with large θ for clinical and research studies have not yet been fully explored, it is reminiscent of when fully 3D imaging was becoming more

Figure 1. (a) Schematic showing the axial acceptance angle (θ) and accepted lines of response that increase from a standard AFOV (shaded) to a long AFOV in a TB-PET system. Geometric axial sensitivity profiles for a 200 cm long central line source (b) in air and attenuated by (c) 20 cm and (d) 35 cm cylinders for AFOVs ranging from 26 to 200 cm. Note the change in y-axis scales for the attenuated profiles. The gains in peak sensitivity relative to a 26 cm AFOV system for the source in a 20 cm cylinder are 1.8x, 2.0x, 2.0x, and 2.0x for 70-, 100-, 140-, and 200 cm AFOV, respectively; the gains in total sensitivity relative to a 26 cm AFOV system for the source in a 20 cm cylinder are 5.9x, 10.1x, 16.0x, and 25.0x for 70-, 100-, 140-, and 200 cm AFOV, respectively. The sensitivity gains are higher for the source in air and slightly lower for the source in the 35 cm cylinder (Courtesy, Dr S. Surti). AFOV, axial field of view; TB-PET, total body positron emission tomography.

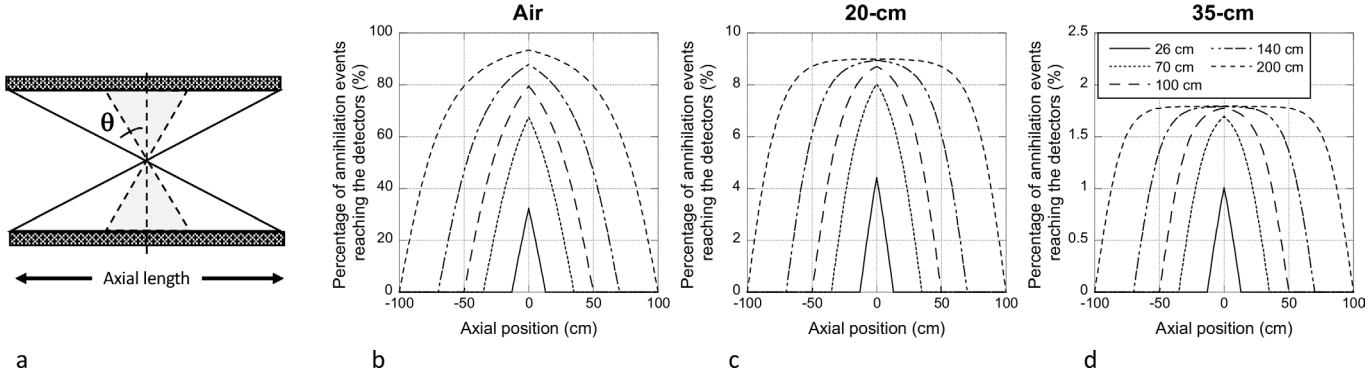

widely used in the 1990s—ultimately the large gains from sensitivity were favored over the small losses of spatial resolution, which were mitigated by more accurate 3D reconstruction algorithms.[11]

Performance measurements

Performance standards (*e.g.* NEMA NU-2 PET standard[12]) to characterize intrinsic and overall system performance are intended to be straightforward, and, while they may not mimic clinical studies, their results are indicative of scanner behavior in the clinic. TB-PET systems, however, are longer than the 65 cm maximum length envisioned in the early 2000s when the NEMA whole-body PET standard was first developed,[13] and some of these measurements will not reflect TB-PET system performance. For example, because the axial spatial resolution may vary across the AFOV, measurements of the spatial resolution at an additional position in between the two axial positions currently specified (center of the AFOV and 3/8 of the AFOV from the center) would better characterize system performance in the clinic.

The sensitivity measurement in the NEMA PET standard specifies a 70 cm long line source; UC-Davis and UPenn have reported sensitivity using both a 70 cm long source (for comparison with standard AFOV systems) and a 170 cm long source.[1,2] A length of 170 cm was chosen to match the average height of an adult human,[14] noting that for a shorter scanner the activity outside the FOV has no effect, but for a longer scanner (*e.g.* the uEXPLORER) the scanner sensitivity will not be fully characterized. Since the sensitivity measurement (line source in air) is not a realistic measurement for patient imaging, but is used to characterize intrinsic performance, we think that a line source equal to or greater than the TB-PET scanner AFOV may be best. To compare the sensitivity measurement with that of conventional scanners, the central 70 cm of the axial sensitivity profile can be summed with the activity/cm scaled to that used for the 70 cm NEMA specification. In this way the measurement for conventional scanners does not need to change.

A similar argument can be made for increasing the length of the count rate performance phantom, where the NEMA PET standard calls for using a 70 cm long line in a 20 cm diameter phantom of the same length. There is some merit in this shorter phantom, since most organs of interest (brain to pelvis) are within ~70–100 cm even though the activity at high concentrations may be locally distributed (*e.g.* a bolus in the heart) or distributed through more of the body, depending on the radiotracer. Measurements with longer phantoms, ranging from 140 cm[15] to 175 cm[1] have been reported to characterize a wider range of imaging scenarios that can be instructive in predicting performance in the clinic.

The remaining NEMA PET performance measurements are generally applicable to TB-PET systems. It can be instructive, though, to measure the image quality phantom (length: 18 cm) in both the axial center and closer to an end of the AFOV (as done in Spencer et al[1]) to characterize the behavior of the clinical reconstruction algorithm and accuracy of corrections throughout the system and capture the impact of changes in axial spatial resolution on contrast recovery.

Considerations with TB-PET systems

There are several factors associated with imaging on a TB-PET system that are not usually encountered on standard AFOV PET scanners. TB-PET systems stress the computational system due to the very large data sizes associated with these devices. With an unrestricted axial acceptance angle, the number of possible lines of response (LORs) increases roughly as the square of the AFOV: while a single ring of the PennPET Explorer (22.9 cm AFOV) would have 2.9×10^8 LORs, the full 6-ring system (142 cm AFOV) has 1.0×10^{10} and requires 1 TB to store a 60 min [^{18}F]-fludeoxyglucose (FDG) dynamic scan (370 MBq injection). Both the uEXPLORER and Quadra systems restrict the axial acceptance angle, so the number of accepted LORs is less. In addition, in order to accept all true coincidences with the largest acceptance angle (and largest potential TOF difference), the coincidence timing window must be extended, which leads to increased random coincidences (and scatter), although this may be optimized by allowing the timing window to vary with axial angle, as is done on the uEXPLORER.[1] Reconstruction times also increase with the large data sizes and the need in dynamic studies to generate multiframe images or 4D parametric images[16–21] to capture the time course of the radiotracer for kinetic modeling of biologic parameters. While a static study can be reconstructed within an hour of acquisition on the PennPET Explorer, dynamic studies can take several hours. The reconstructions are faster on commercial systems; a dynamic FDG study on the Quadra, *e.g.* can be reconstructed in under 1 h.

The current default reconstruction algorithm on TB-PET systems is fundamentally the same as on most standard PET scanners: TOF iterative reconstruction based on the ordered subsets expectation maximization (OSEM) algorithm[22,23] that can include modeling of the point spread function (PSF).[24] The PSF model should include the axial dependence of the axial resolution, in addition to the usual radial dependence of transverse resolution. The accuracy of the corrections for attenuation, detector normalization, and random and scattered events must also be carefully considered on a TB-PET system, since the magnitude of these corrections becomes larger with longer AFOV. Attenuation factors (derived from CT) and detector normalization correction factors vary substantially with axial angle; in addition, a measurement of normalization factors requires a longer acquisition time to ensure adequate counts are collected for all LORs to avoid propagation of noise in the correction factors into the reconstructed image.[25] As with standard AFOV scanners, random events are accurately estimated with a delayed coincidence window; the higher randoms fractions with larger axial acceptance angle can, however, increase image noise. Finally, the number of detected scattered events also increases with AFOV and can increase image noise as well even if accurately estimated. Despite the challenges of adapting standard methods for data correction and image reconstruction to the larger data sets, TB-PET systems generate quantitatively accurate images on par with standard AFOV systems, as evidenced by careful phantom and validation studies (*e.g. references3,4*).

There are also practical challenges with TB-PET, for both patient and investigator. One obvious difference is the length of the tunnel, which can reduce access to the patient and increase the possibility of claustrophobia and patient motion. This demands that care is taken in the design of lighting, air flow, and patient–staff communication. The Siemens Quadra has the shortest AFOV and the largest bore, thereby minimizing these effects, whereas the PennPET Explorer is unique in having an open space between the PET and CT portions of the system that allows for ready access to the patient. This is especially helpful for research studies when blood sampling is required or when radiotracer is injected while the patient is being imaged. It is still important to keep the tubing as short as possible (*e.g.* 1 m or shorter) to minimize dead space (delays) and dispersion in the tubing. Also, unlike standard AFOV scanners, the tubing is within the FOV of the system; for early frames following a bolus injection or for studies involving a continuous infusion of activity, the presence of focal activity outside the body can lead to errors in the scatter estimate unless properly handled. Another distinction of TB-PET systems is the design of the patient bed that must handle the long (~2 m) travel to ensure no or fixed deflection differences between the CT and all parts of the PET system. It should be noted that all standard AFOV systems allow for long travel to image the whole body, albeit in multiple bed positions, but the distance between the CT and the PET is shorter for these systems, so variable deflection is less of a concern. Finally, the room size or layout of the system in the room can be an issue for longer systems.

FUTURE DIRECTIONS

The first generation of TB-PET systems has demonstrated the benefits of these systems and shown that TB-PET systems are reliable, based on feedback from users, despite the large increase in the number of components. Since current TB-PET systems are based on technology that was adapted from standard systems, it is expected that further advances in detector technology or data processing methods could be translated to TB-PET systems to improve their system performance as well. This might include detector materials or SiPMs to improve TOF resolution or monolithic (or semi-monolithic) detectors with DOI capability, which are under investigation to improve the spatial resolution without the need for ever smaller crystal elements.[26,27] For TB-PET, there is also a priority to reduce their cost (which roughly scales with axial length and is, therefore, 3–6 times that of a standard AFOV system) to allow wider dissemination of these systems. Given the high cost of the LSO or L(Y)SO scintillator, one might reduce the crystal thickness and recover effective sensitivity with improved TOF resolution.[28] Alternatively, lower cost scintillators may be used. A prototype TOF PET system using low-cost plastic scintillation detectors is under development,[29] although this system will have lower sensitivity than one based on lutetium-based detectors (while still higher than standard AFOV systems). Another technology under development is TOF detectors based on measurement of the Cerenkov radiation in bismuth germanate (BGO) detectors,[30,31] which might eventually offer a lower-cost alternative for TB-PET.

System geometry design is one area where there is potential to achieve most of the benefits of TB-PET with a lower total cost. Reducing the number of detectors, through axial gaps between detector rings or "missing" detectors both within a ring and between rings, can allow for long axial coverage but at the cost of some of the sensitivity gain achieved with complete detector coverage.[32–35] Sparse detector designs take advantage of the redundancy of data used in 3D reconstruction. In fact, the PennPET Explorer has demonstrated the utility of a sparse detector geometry for TB-PET, operating until recently with interring gaps equal to 30% of the active detector length; this affected the overall sensitivity, but not image uniformity or quantitative accuracy. For many applications, the trade-off of sensitivity is offset by the longer axial coverage (for fixed number of detectors) and still very large sensitivity gain.

There are also several developments in image reconstruction underway that will take advantage of the long AFOV or complement the benefits of TB-PET. Four-dimensional reconstruction of dynamic processes is enabled by the simultaneous coverage of the whole body and the high sensitivity of the system that permits ultra-fast (<1 s) temporal sampling.[16] Deep learning-based reconstruction (*e.g.* Gong et al[36]) or post-processing has the potential to reduce the difficulties of handling the large data sets and to improve low-count images. Pediatric or serial studies (where the high sensitivity of a long AFOV systems permits low injected activities) will be enabled by joint emission/attenuation estimation using algorithms[37–39] to reduce the radiation exposure further by eliminating the CT scan.

CLINICAL APPLICATIONS

In the few years since their development, TB-PET scanners have already demonstrated the clinical benefits due to the increased sensitivity. Both the uEXPLORER and Quadra are routinely used as clinical instruments, as well as for research investigations, whereas the PennPET Explorer is currently a dedicated research instrument, although clinical protocols can be performed in the context of research with informed consent by the patient.

The initial human studies of healthy subjects on the uEXPLORER demonstrated exquisite detail in the PET images with longer scan durations (up to 20 min), including vessel walls, spinal cord, and brain, whereas imaging with very short scan durations (<1 min) yielded satisfactory PET images, as did imaging with very low administered doses (25 MBq).[4] Currently, on a uEXPLORER at Zhongshan Hospital, three protocols are used for FDG PET. The first choice is a low-dose protocol with 1.85 MBq/kg and a 3–5 min scan, but this may be increased to 3.7 MBq/kg with scans 0.5–2 min, or decreased to 0.37 MBq/kg with scans 7–15 min, depending on the patient, disease, and clinical question.[5] In contrast, at UC Davis, a clinical protocol for routine FDG scans was chosen using 296 MBq (8 mCi) with 20 min scans at 2 h post-injection (p.i.), designed to optimize image quality and to enhance lesion contrast.[40] For lymphoma patients, imaging is also performed at 1 hour p.i. so that the Deauville criteria can be applied, using the 5-point scale to compare uptake in sites of disease to blood pool uptake in the mediastinum and uptake in undiseased liver parenchyma.[41] Given washout of tracer from both structures over time, such studies show that imaging at 2 h may give a different classification than at 1 h. Similarly, the

increased image quality of TB-PET may reveal sites of uptake that may not be visualized on conventional PET/CT, such as normal subcentimeter cervical lymph nodes.[42] The interpreting physician should be aware of such differences in image quality and adjust their interpretation accordingly, understanding typical patterns of disease. It is notable that both Zhongshan Hospital and UC Davis have demonstrated improved clinical benefit with the uEXPLORER, but with different imaging protocols, underscoring the ability to tailor imaging studies to clinical needs.

Although the PennPET Explorer is not used routinely for clinical imaging, a number of clinical patients with disease have been imaged in a back-to-back comparison to clinical scanners with standard AFOVs. Even in its initial configuration with a 64 cm AFOV, qualitatively superior images were obtained on the PennPET Explorer compared to the standard scan for the same scanning duration (~16 min), whereas very short scans (~2 min) yielded comparable quality images to the standard scan.[6] Imaging with the current configuration of 142 cm AFOV indicates that a 5 min scan (at 60 min p.i.) provides excellent diagnostic quality for adults, with 370 MBq (10 mCi) injected dose. A pediatric protocol utilizes similarly short scans, but with a weight-based injected dose, thereby minimizing patient motion and obviating the need for anesthesia with its inherent risks in children.[43] Imaging with low-dose protocols for both PET and CT will also benefit this patient population where cumulative radiation exposure is a concern.[44]

A larger head-to-head study was performed between the Quadra and a Biograph Vision PET/CT (26.3 cm AFOV) with FDG, ^{18}F-PSMA, and ^{68}Ga-DOTATATE. Compared to a 16 min scan on the standard AFOV, the Quadra achieved equivalent target lesional integral activity and signal-to-noise in less than 2 min; 10 min images on the Quadra, though, were clearly superior, and guided the current clinical protocol of 6–10 min scan duration. As an alternative to shorter scans, these investigators also calculated that an injected dose of under 40 MBq (~1 mCi) may be used with satisfactory image quality,[7] again underscoring the increased flexibility with TB-PET to tailor protocols to clinical needs.

Other studies demonstrated the increased sensitivity for detection of disease compared to conventional PET. In a patient with metastatic colon cancer, the PennPET Explorer demonstrated a supradiaphragmatic lymph node that was not seen on standard PET.[6] It is noted that later images benefit from increased trapping of FDG in malignancy with washout from normal tissue, but also that the high sensitivity of TB-PET scanners compensates for the loss of signal due to radioactive decay. In a more striking example, in a patient with a metastatic neuroendocrine tumor, ^{68}Ga-DOTATATE PET images on the PennPET Explorer provided comparable diagnostic information to the standard scan, although images were obtained on the PennPET Explorer 3.5 hours p.i. Such protocols may prove especially useful for tracers with production difficulties, such as generator-produced ^{68}Ga-DOTATATE with a relatively short half-life of 68 min.[45] The increased sensitivity of TB-PET can also be leveraged for imaging neuroendocrine tumors with ^{64}Cu-DOTATATE, which has recently been FDA approved with increased clinical availability secondary to a 12.7 h half-life and cyclotron production.[46] ^{64}Cu, though, has a relatively low positron branching ratio (17.5%) compared to ^{68}Ga (89%),[47] necessitating different imaging protocols to optimize clinical imaging with each of these tracers.

Early clinical experience with each available TB-PET has clearly demonstrated the added value and increased flexibility of imaging with these sensitive instruments: image quality is significantly improved using similar scan time and injected dose as standard AFOV instruments, but the increased sensitivity of TB-PET can be leveraged to enable imaging faster, with lower injected dose, and with delayed scan start times to enhance lesion contrast. With increasing experience, clinical uses will continue to evolve with the imaging protocols tailored to particular clinical applications.

RESEARCH APPLICATIONS

Clearly, TB-PET scanners add value in the current clinical space, but these powerful scanners also have the ability to truly advance the field by creating new opportunities in PET imaging and ushering in a new era of precision medicine. Many research projects have been initiated with these instruments with early results demonstrating promise.

Delayed imaging to characterize tumor biology

As discussed above, TB-PET scanners have demonstrated the ability to image at delayed time points after injection to improve clinical diagnostics. Delayed imaging can also benefit research studies by better characterizing tracer biology. In a dramatic illustration of this, imaging as late as 24 hours p.i. of a standard injected dose of FDG demonstrated washout of tracer from the brain at delayed time points. This provided definitive evidence supporting what had earlier been suspected about the kinetics of FDG in the brain, but not as definitely shown.[6] Similarly, images of a ^{89}Zr-labelled anti-CD8 minibody obtained at 24 h on the PennPET Explorer demonstrated the ability to track immune cells over time.[48] With relatively slow temporal changes in the activity distribution and a 23% positron faction,[49] these ongoing studies benefit greatly from the extended axial length and high sensitivity of the PennPET Explorer, since they require low injected dose (~37 MBq) to minimize the radiation dose to normal tissues.

TB-PET to optimize dosimetry estimates to guide radionuclide therapy

In a more novel application of delayed imaging, TB-PET can be utilized to provide reliable estimates of radiation dosimetry to better guide radionuclide therapy. Currently, the use of radiation dosimetry to guide therapy is limited to planar imaging in clinical nuclear medicine. Dosimetry is only routinely used to determine a maximum tolerated administered activity in patients with metastatic thyroid cancer treated with radioactive iodine therapy[50] and to modify the cumulative administered activity of high specific activity of ^{131}I-iobenguane in the treatment of advanced pheochromocytoma or paraganglioma.[51] Notably, treatment of neuroendocrine tumors with ^{177}Lu-DOTATATE

Figure 2. Representative maximum intensity projection images from studies on the PennPET Explorer that demonstrate the multiple benefits of TB-PET systems with a range of AFOV. Images are shown for a (a) dynamic ^{18}F-FDG study in a 3-ring (64 cm) configuration, (b) dynamic ^{18}F-FDG study in a 6-ring (142 cm) configuration (courtesy, Dr C. Wiers), and (c) ^{89}Zr-CD8 study in a 5-ring (112 cm) configuration, acquired in two bed positions to scan the 1.83 m tall subject (courtesy, Dr M. Farwell). The different temporal framing for (a) and (b) reflects the different goals of these two studies. The positioning of the subject was adjusted for each study to place the axial region of interest more centrally in the AFOV. AFOV, axial field of view; ^{18}F-FDG, 18-fluorodeoxyglucose; TB-PET, total body positron emission tomography.

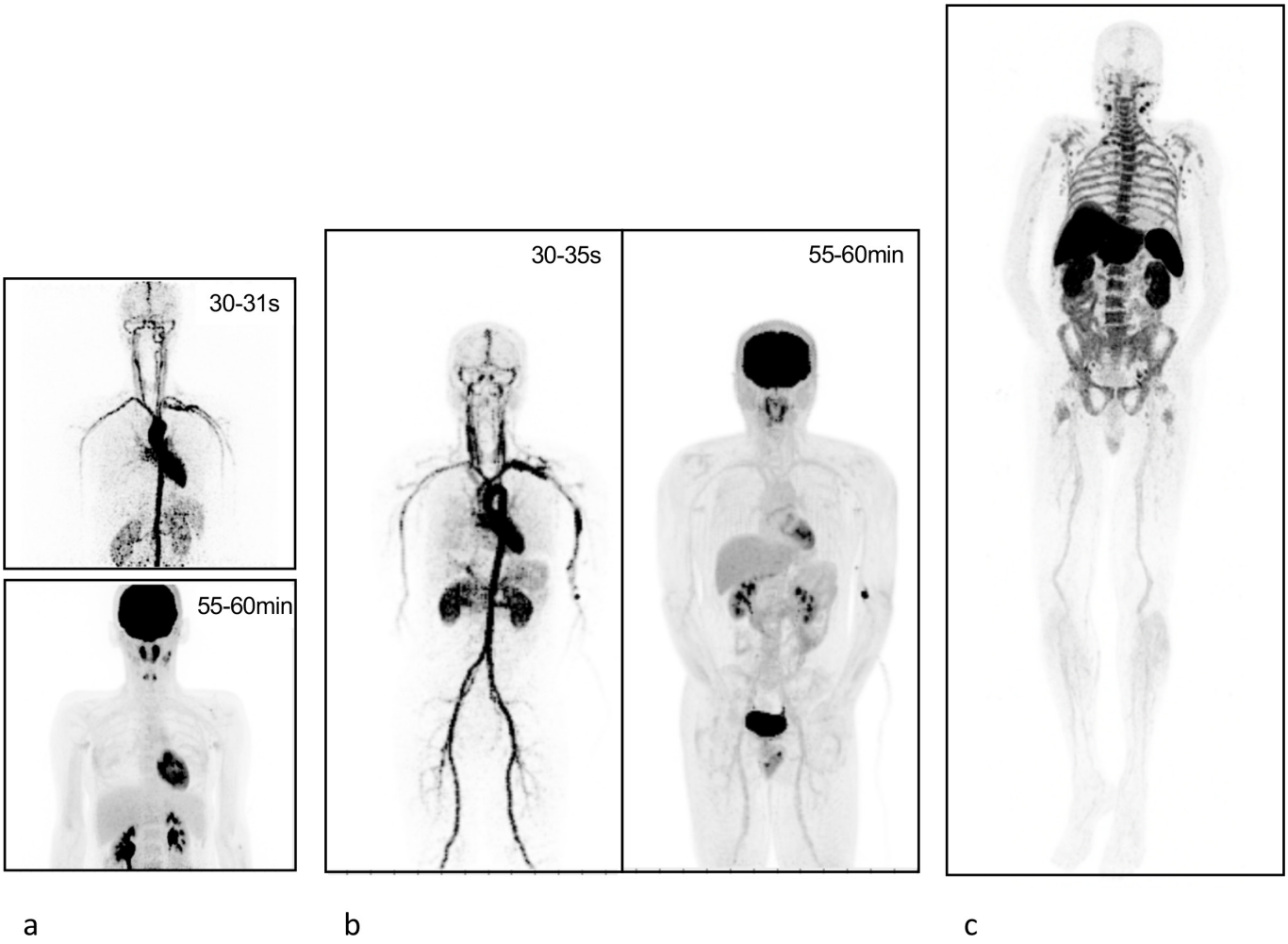

does not utilize dosimetry data for determination of injected activity. Rather, a fixed dose of 7.4 GBq (200 mCi) is administered for four total doses unless modified by patient factors, usually a decline in blood counts from hematotoxicity.[52] A companion diagnostic DOTATATE PET scan is most often used to select patients for therapy based on a shared target with ^{177}Lu-DOTATATE, but is not utilized for dosimetric purposes. Similarly, ^{177}Lu-vipivotide tetraxetan, approved in March 2022 for treatment of certain patients with PSMA-positive metastatic castration-resistant prostate cancer, has a companion diagnostic PET scan to select patients for therapy, but likewise does not utilize dosimetry for determination of injected dose.[53]

The imprecision of currently utilized dosimetry methods hampers research into dosimetry-guided radionuclide treatment and ultimate clinical adoption. The narrow therapeutic window of most radiopharmaceuticals necessitates precision that cannot be attained with planar or SPECT methods. While SPECT/CT may achieve reasonable estimates of whole organ dose, it cannot accurately determine tumor dose, since SPECT suffers from suboptimal contrast recovery and increased variability. It is difficult to envision clinically useful dosimetry if it does not provide tumor dose estimates to understand the likely benefit of therapy. TB-PET provides an alternative to these methods, as evidenced by the ability to image PET tracers at delayed time points. This ability to precisely measure the tail of the time activity curve may provide data necessary to advance this research area. This ability is not limited to large homogeneous areas of activity, as the spatial resolution and contrast recovery allow accurate and precise measurements of both small lesions and suborgan heterogeneity (*e.g.* activity within renal cortex versus collecting systems). Specifically, ^{64}Cu-DOTATATE[46] may be leveraged for dosimetry estimates to guide treatment with ^{177}Lu-DOTATATE.

Dual-tracer imaging with TB-PET

In just the past decade, several radiotracers have advanced into the nuclear medicine clinic (^{18}F-Fluciclovine, ^{18}F-DCFPyL, ^{68}Ga-PSMA, ^{18}F-Fluoroestradiol, ^{68}Ga-DOTATATE, ^{64}Cu-DOTATATE), improving the ability to stage and characterize disease. These clinical tracers complement a growing array of investigational PET agents. However, characterizing malignancy fully with different radiotracers is hampered by the need to allow for radioactive decay between scans (*e.g.* 1 day with ^{18}F). This limits the ability to characterize tumor biology in a single imaging session and impedes recruitment efforts to clinical trials. By leveraging the sensitivity advantages of TB-PET, we have developed dual-tracer imaging on the PennPET Explorer using two tracers: ^{18}F-FDG and ^{18}F-Fluoroglutamine as measures of glucose and glutamine metabolism, respectively. An initial ^{18}F-Fluoroglutamine (FGln) study with a research subject with breast cancer demonstrated that the volume of distribution (V_D) of FGln, the kinetic parameter of interest, can be accurately estimated in 30 min with an injected dose of 37 MBq (1 mCi) because of the high sensitivity of the PennPET Explorer. Based on these results, a second subject was injected with 37 MBq of FGln and imaged for 30 min followed by an injection of 370 MBq (10 mCi) of FDG, which allowed the calculation of both V_D for FGln and FDG delivery and flux in the same imaging session. Of course, this paradigm could be extended to other tracers, including clinical tracers that are imaged at late static time points (*e.g.* ^{18}F-Fluoroestradiol or ^{18}F-Fluorothimidine and FDG). TB-PET may enable "multiparametric" PET, expanding the potential of molecular imaging.[54]

SUMMARY

The studies performed in the last several years with the first-generation systems, which have ranged in AFOV from 64 to 194 cm, serve to illustrate the trade-offs made between AFOV and performance. Figure 2 shows three examples of studies performed with the PennPET Explorer in configurations with different AFOV. The first study illustrates that even a 64 cm AFOV permits multiorgan dynamic imaging with a measured input function and sufficient sensitivity to permit time frames as short as 1 s. This shorter AFOV is also sufficient for organ-focused studies, such as those of the brain or heart, which benefit from the higher axial sensitivity of a TB-PET system. The second study was performed more recently with the full 142 cm AFOV and illustrates the advantage of capturing all major organs with greater flexibility in positioning for tall patients. Both subjects for these studies were 176 cm. The third study was performed earlier with 112 cm AFOV and required a 2-bed scan since the subject was 183 cm, and the study was designed to detect inflammation in the legs as well as upper body. Such studies performed with a static radiotracer uptake are feasible with multiple bed positions, but also extend the total scan duration if the AFOV is not long enough to capture the full area of interest. The "optimal" AFOV therefore does not exist; instead, the most suitable AFOV is task-specific and depends on the intended application(s) of the system. Clearly, from the early work described, all TB-PET scanners with AFOV>60 cm offer significant benefits for many clinical and research applications, and we anticipate that the applications will grow as an expanding base of users gains additional experience with these new systems. These higher sensitivity systems will enable radiotracer development, expanding the field beyond FDG to new tracers better matched to specific diseases or conditions.

CONFLICTS OF INTEREST

MD-W has no conflicts to report. ARP has received consulting fees from Progenics and Blue Earth Diagnostics. DAP has received research funding from Siemens Healthineers, Progenics, Nordic Nanovector, Fusion Pharmaceuticals, Point Biopharma, 511 Pharma, and consulting fees from Siemens, Lantheus, Actinum, and Bayer. JSK has received research funding from Siemens Healthineers.

REFERENCES

1. Spencer BA, Berg E, Schmall JP, Omidvari N, Leung EK, Abdelhafez YG, et al. Performance evaluation of the uexplorer total-body PET/CT scanner based on NEMA NU 2-2018 with additional tests to characterize PET scanners with a long axial field of view. *J Nucl Med* 2021; **62**: 861–70. https://doi.org/10.2967/jnumed.120.250597
2. Karp JS, Viswanath V, Geagan MJ, Muehllehner G, Pantel AR, Parma MJ, et al. PennPET explorer: design and preliminary performance of a whole-body imager. *J Nucl Med* 2020; **61**: 136–43. https://doi.org/10.2967/jnumed.119.229997
3. Prenosil GA, Sari H, Fürstner M, Afshar-Oromieh A, Shi K, Rominger A, et al. Performance characteristics of the biograph vision quadra PET/CT system with a long axial field of view using the NEMA NU 2-2018 standard. *J Nucl Med* 2022; **63**: 476–84. https://doi.org/10.2967/jnumed.121.261972
4. Badawi RD, Shi H, Hu P, Chen S, Xu T, Price PM, et al. First human imaging studies with the explorer total-body PET scanner. *J Nucl Med* 2019; **60**: 299–303. https://doi.org/10.2967/jnumed.119.226498
5. Sui X, Liu G, Hu P, Chen S, Yu H, Wang Y, et al. Total-body PET/computed tomography highlights in clinical practice: experiences from zhongshan hospital, fudan university. *PET Clin* 2021; **16**: 9–14. https://doi.org/10.1016/j.cpet.2020.09.007
6. Pantel AR, Viswanath V, Daube-Witherspoon ME, Dubroff JG, Muehllehner G, Parma MJ, et al. PennPET explorer: human imaging on a whole-body imager. *J Nucl Med* 2020; **61**: 144–51. https://doi.org/10.2967/jnumed.119.231845
7. Alberts I, Hünermund J-N, Prenosil G, Mingels C, Bohn KP, Viscione M, et al. Clinical performance of long axial field of view PET/CT: a head-to-head intra-individual comparison of the biograph vision quadra with the biograph vision PET/CT. *Eur J Nucl Med Mol Imaging* 2021; **48**: 2395–2404. https://doi.org/10.1007/s00259-021-05282-7
8. Conti M. Focus on time-of-flight PET: the benefits of improved time resolution. *Eur J Nucl Med Mol Imaging* 2011; **38**: 1147–57. https://doi.org/10.1007/s00259-010-1711-y
9. Surti S, Pantel AR, Karp JS. Total body PET: why, how, what for? *IEEE Trans Radiat Plasma Med Sci* 2020; **4**: 283–92. https://doi.org/10.1109/trpms.2020.2985403

10. Schmall JP, Karp JS, Werner M, Surti S. Parallax error in long-axial field-of-view PET scanners-a simulation study. *Phys Med Biol* 2016; **61**: 5443–55. https://doi.org/10.1088/0031-9155/61/14/5443
11. Kinahan PE, Karp JS. Figures of merit for comparing reconstruction algorithms with a volume-imaging PET scanner. *Phys Med Biol* 1994; **39**: 631–42. https://doi.org/10.1088/0031-9155/39/3/024
12. NEMA. *NEMA standards publication NU 2-2018: Performance measurements of positron emission tomographs*. Rosslyn VA, USA: National Electrical Manufacturers Association; 2018.
13. Daube-Witherspoon ME, Karp JS, Casey ME, DiFilippo FP, Hines H, Muehllehner G, et al. PET performance measurements using the NEMA NU 2-2001 standard. *J Nucl Med* 2002; **43**: 1398–1409.
14. McDowell MA, Fryar CD, Ogden CL, Flegal KM. Anthropometric reference data for children and adults: United states, 2003–2006. *Natl Health Stat Report* 2008; **10**: 1–48.
15. Viswanath V, Daube-Witherspoon ME, Pantel AR, Parma MJ, Werner ME, Karp JS. Performance benefits of extending the AFOV of PET scanners. 2020 IEEE Nuclear Science Symposium and Medical Imaging Conference (NSS/MIC); Boston, MA, USA. Piscataway, NJ: IEEE; 2020. https://doi.org/10.1109/NSS/MIC42677.2020.9507858
16. Zhang X, Xie Z, Berg E, Judenhofer MS, Liu W, Xu T, et al. Total-body dynamic reconstruction and parametric imaging on the uexplorer. *J Nucl Med* 2020; **61**: 285–91. https://doi.org/10.2967/jnumed.119.230565
17. Rahmim A, Tang J, Zaidi H. Four-dimensional (4d) image reconstruction strategies in dynamic PET: beyond conventional independent frame reconstruction. *Med Phys* 2009; **36**: 3654–70. https://doi.org/10.1118/1.3160108
18. Reader AJ, Verhaeghe J. 4D image reconstruction for emission tomography. *Phys Med Biol* 2014; **59**: R371–418. https://doi.org/10.1088/0031-9155/59/22/R371
19. Wang G, Qi J. Direct estimation of kinetic parametric images for dynamic PET. *Theranostics* 2013; **3**: 802–15. https://doi.org/10.7150/thno.5130
20. Kamasak ME, Bouman CA, Morris ED, Sauer K. Direct reconstruction of kinetic parameter images from dynamic PET data. *IEEE Trans Med Imaging* 2005; **24**: 636–50. https://doi.org/10.1109/TMI.2005.845317
21. Wang G, Qi J. Generalized algorithms for direct reconstruction of parametric images from dynamic PET data. *IEEE Trans Med Imaging* 2009; **28**: 1717–26. https://doi.org/10.1109/TMI.2009.2021851
22. Parra L, Barrett HH. List-mode likelihood: EM algorithm and image quality estimation demonstrated on 2-D PET. *IEEE Trans Med Imaging* 1998; **17**: 228–35. https://doi.org/10.1109/42.700734
23. Hudson HM, Larkin RS. Accelerated image reconstruction using ordered subsets of projection data. *IEEE Trans Med Imaging* 1994; **13**: 601–9. https://doi.org/10.1109/42.363108
24. Panin VY, Kehren F, Michel C, Casey M. Fully 3-D PET reconstruction with system matrix derived from point source measurements. *IEEE Trans Med Imaging* 2006; **25**: 907–21. https://doi.org/10.1109/tmi.2006.876171
25. Zhang X, Zhou J, Cherry SR, Badawi RD, Qi J. Quantitative image reconstruction for total-body PET imaging using the 2-meter long EXPLORER scanner. *Phys Med Biol* 2017; **62**: 2465–85. https://doi.org/10.1088/1361-6560/aa5e46
26. Stockhoff M, Decuyper M, Van Holen R, Vandenberghe S. High-resolution monolithic LYSO detector with 6-layer depth-of-interaction for clinical PET. *Phys Med Biol* 2021; **66**(15). https://doi.org/10.1088/1361-6560/ac1459
27. Borghi G, Tabacchini V, Bakker R, Schaart DR. Sub-3 mm, near-200 ps TOF/DOI-PET imaging with monolithic scintillator detectors in a 70 cm diameter tomographic setup. *Phys Med Biol* 2018; **63**(15): 155006. https://doi.org/10.1088/1361-6560/aad2a6
28. Surti S, Werner ME, Karp JS. Study of PET scanner designs using clinical metrics to optimize the scanner axial FOV and crystal thickness. *Phys Med Biol* 2013; **58**: 3995–4012. https://doi.org/10.1088/0031-9155/58/12/3995
29. Moskal P, Kowalski P, Shopa RY, Raczyński L, Baran J, Chug N, et al. Simulating NEMA characteristics of the modular total-body J-PET scanner-an economic total-body PET from plastic scintillators. *Phys Med Biol* 2021; **66**(17). https://doi.org/10.1088/1361-6560/ac16bd
30. Kwon SI, Gola A, Ferri A, Piemonte C, Cherry SR. Bismuth germanate coupled to near ultraviolet silicon photomultipliers for time-of-flight PET. *Phys Med Biol* 2016; **61**: L38–47. https://doi.org/10.1088/0031-9155/61/18/L38
31. Brunner SE, Schaart DR. BGO as a hybrid scintillator / cherenkov radiator for cost-effective time-of-flight PET. *Phys Med Biol* 2017; **62**: 4421–39. https://doi.org/10.1088/1361-6560/aa6a49
32. Zein SA, Karakatsanis NA, Conti M, Nehmeh SA. Monte carlo simulation of the siemens biograph vision PET with extended axial field of view using sparse detector module rings configuration. *IEEE Trans Radiat Plasma Med Sci* 2021; **5**: 331–42. https://doi.org/10.1109/TRPMS.2020.3034676
33. Yamaya T, Yoshida E, Inadama N, Nishikido F, Shibuya K, Higuchi M, et al. A multiplex "openpet" geometry to extend axial FOV without increasing the number of detectors. *IEEE Trans Nucl Sci* 2009; **56**: 2644–50. https://doi.org/10.1109/TNS.2009.2027437
34. Daube-Witherspoon ME, Viswanath V, Werner ME, Karp JS. Performance characteristics of long axial field-of-view PET scanners with axial gaps. *IEEE Trans Radiat Plasma Med Sci* 2021; **5**: 322–30. https://doi.org/10.1109/trpms.2020.3027257
35. Vandenberghe S, Moskal P, Karp JS. State of the art in total body PET. *EJNMMI Phys* 2020; **7**: 35. https://doi.org/10.1186/s40658-020-00290-2
36. Gong K, Berg E, Cherry SR, Qi J. Machine learning in PET: from photon detection to quantitative image reconstruction. *Proc IEEE* 2019; **108**: 51–68. https://doi.org/10.1109/JPROC.2019.2936809
37. Li Y, Matej S, Karp JS. Practical joint reconstruction of activity and attenuation with autonomous scaling for time-of-flight PET. *Phys Med Biol* 2021; **65**: 235037. https://doi.org/10.1088/1361-6560/ab8d75
38. Rezaei A, Defrise M, Nuyts J. ML-reconstruction for TOF-PET with simultaneous estimation of the attenuation factors. *IEEE Trans Med Imaging* 2014; **33**: 1563–72. https://doi.org/10.1109/TMI.2014.2318175
39. Defrise M, Rezaei A, Nuyts J. Time-of-flight PET data determine the attenuation sinogram up to a constant. *Phys Med Biol* 2012; **57**: 885–99. https://doi.org/10.1088/0031-9155/57/4/885
40. Nardo L, Abdelhafez YG, Spencer BA, Badawi RD. Clinical implementation of total-body PET/CT at university of california, davis. *PET Clin* 2021; **16**: 1–7. https://doi.org/10.1016/j.cpet.2020.09.006
41. Meignan M, Gallamini A, Meignan M, Gallamini A, Haioun C. Report on the first international workshop on interim-PET-scan in lymphoma. *Leuk Lymphoma* 2009; **50**: 1257–60. https://doi.org/10.1080/10428190903040048
42. Nardo L, Pantel AR. Oncologic applications of long axial field-of-view PET/computed tomography. *PET Clin* 2021; **16**: 65–73. https://doi.org/10.1016/j.cpet.2020.09.010
43. Arlachov Y, Ganatra RH. Sedation/anaesthesia in paediatric radiology. *Br J Radiol* 2012; **85**: 31. https://doi.org/10.1259/bjr/28871143

44. Chawla SC, Federman N, Zhang D, Nagata K, Nuthakki S, McNitt-Gray M, et al. Estimated cumulative radiation dose from PET/CT in children with malignancies: a 5-year retrospective review. *Pediatr Radiol* 2010; **40**: 681–86. https://doi.org/10.1007/s00247-009-1434-z
45. Kumar K. The current status of the production and supply of gallium-68. *Cancer Biother Radiopharm* 2020; **35**: 163–66. https://doi.org/10.1089/cbr.2019.3301
46. Pfeifer A, Knigge U, Mortensen J, Oturai P, Berthelsen AK, Loft A, et al. Clinical PET of neuroendocrine tumors using 64cu-DOTATATE: first-in-humans study. *J Nucl Med* 2012; **53**: 1207–15. https://doi.org/10.2967/jnumed.111.101469
47. Conti M, Eriksson L. Physics of pure and non-pure positron emitters for PET: a review and a discussion. *EJNMMI Phys* 2016; **3**: 8. https://doi.org/10.1186/s40658-016-0144-5
48. Farwell MD, Gamache RF, Babazada H, Hellmann MD, Harding JJ, Korn R, et al. CD8-targeted PET imaging of tumor-infiltrating T cells in patients with cancer: A phase I first-in-humans study of ^{89}zr-df-IAB22M2C, A radiolabeled anti-CD8 minibody. *J Nucl Med* 2022; **63**: 720–26. https://doi.org/10.2967/jnumed.121.262485
49. Heskamp S, Raavé R, Boerman O, Rijpkema M, Goncalves V, Denat F. (89)zr-immuno-positron emission tomography in oncology: state-of-the-art (89)zr radiochemistry. *Bioconjug Chem* 2017; **28**: 2211–23.
50. Dorn R, Kopp J, Vogt H, Heidenreich P, Carroll RG, Gulec SA. Dosimetry-guided radioactive iodine treatment in patients with metastatic differentiated thyroid cancer: largest safe dose using a risk-adapted approach. *J Nucl Med* 2003; **44**: 451–56.
51. Pryma DA, Chin BB, Noto RB, Dillon JS, Perkins S, Solnes L, et al. Efficacy and safety of high-specific-activity ^{131}I-MIBG therapy in patients with advanced pheochromocytoma or paraganglioma. *J Nucl Med* 2019; **60**: 623–30. https://doi.org/10.2967/jnumed.118.217463
52. Hope TA, Abbott A, Colucci K, Bushnell DL, Gardner L, Graham WS, et al. NANETS/SNMMI procedure standard for somatostatin receptor–based peptide receptor radionuclide therapy with ^{177}lu-DOTATATE. *J Nucl Med* 2019; **60**: 937–43. https://doi.org/10.2967/jnumed.118.230607
53. Sartor O, de Bono J, Chi KN, Fizazi K, Herrmann K, Rahbar K, et al. Lutetium-177–PSMA-617 for metastatic castration-resistant prostate cancer. *N Engl J Med* 2019; **385**: 1091–1103. https://doi.org/10.1056/NEJMoa2107322
54. Mankoff DA, Pantel AR, Viswanath V, Karp JS. Advances in PET diagnostics for guiding targeted cancer therapy and studying in vivo cancer biology. *Curr Pathobiol Rep* 2019; **7**: 97–108. https://doi.org/10.1007/s40139-019-00202-9